SUSY Hidden in the Continuum

Haiying Cai, Hsin-Chia Cheng, Anibal D. Medina and John Terning

Department of Physics, University of California, One Shields Ave. Davis, CA 95616, USA

October 9, 2013

Abstract

We study models where the superpartners of the ordinary particles have continuous spectra rather than being discrete states, which can occur when the supersymmetric standard model is coupled to an approximately conformal sector. We show that when superpartners that are well into the continuum are produced at a collider they tend to have long decay chains that step their way down through the continuum, emitting many fairly soft standard model particles along the way, with a roughly spherical energy distribution in the center of mass frame.

1 Introduction

In this paper we take the first steps in studying the collider phenomenology of supersymmetric models that have some approximate conformal symmetry, which is reflected in the fact that the superpartners of the standard model (SM) particles have a continuous spectrum [1] rather than being discrete states. The superpartners can have continuous spectra when the supersymmetric standard model is coupled to a conformal field theory (CFT) sector [1] which gives rise to so-called "unparticle" behavior.[1] A mass gap is generated for the superpartners of (and also the excitations of) the SM particles if the conformal symmetry is softly broken in the infrared (IR). This scenario is most easily modeled in a five-dimensional (5D) anti-de Sitter (AdS) space using the AdS/CFT correspondence [6, 7]. The 5D AdS space is cut off by an ultraviolet (UV) brane where supersymmetry (SUSY) is broken. In the absence of an IR brane, the SM fields propagating in the bulk will have continuous spectra. Such a theory would have been ruled out if the spectra continue down to zero mass. However, a mass gap for nonzero-modes can be generated by introducing a soft wall in the IR, which can be parameterized by a position dependent bulk mass term or a dilaton field with an appropriate profile. The boundary conditions on the UV brane remove half of the fermion zero-modes so that the SM chiral fermions can be obtained. In the supersymmetric limit, the 4D theory consists of SM particles and their superpartners as the zero-modes, plus a continuum of Kaluza-Klein (KK) excitations starting from some gap for each field. After SUSY breaking is introduced on the UV brane, the zero modes of the superpartners are lifted while the mass gaps of the continuum excitations are not affected since they are determined in the IR. Depending on the parameters, for large enough SUSY breaking the zero mode of the superpartner can merge into the continuum and only a continuous spectrum for the superpartner is left.

As one can imagine, the collider phenomenology could be quite complicated with continuous spectra. Calculations of production cross-sections have already been dis-

[1] Unparticles are fields with a continuous spectrum [2, 3], possibly with a with a mass gap [4, 5], whose two point functions exhibit a nontrivial scaling behavior.

cussed in [5], so here we will focus on decay processes. Imagine that some highly excited mode in the gluino continuum is produced at the Large Hadron Collider (LHC), it can decay to a squark with an arbitrary mass in the continuum between the squark gap and the initial gluino mass (neglecting the mass of the emitted quark). The squark can then decay back to a gluino as long as the squark mass is above the gluino gap. An obvious question is: does a continuum decay prefer to occur for small mass differences or large mass differences? If the gluino prefers to decay to a squark with an invariant mass close to its own, then the jet emitted in the decay will carry a relatively small amount of energy, and there will be many steps of decays before it reaches the bottom of the spectrum. The events will contain a high multiplicity of soft visible particles, which can be quite challenging at hadron colliders. On the other hand, if the gluino prefers to decay to the squark near the bottom of the spectrum, then we expect only a few decay steps and hard jets from the decays. The signal events in this case are more like traditional SUSY models. Since the theory becomes conformal at high energies, we expect that in the high invariant mass limit we will be closer to the first picture [8–11]. Here we would like to make some more quantitative statements.

Explicit calculations for continuum superpartner events, however, are not straightforward. Because the initial and/or final states are not particles, the usual Feynman rules for particles are not directly applicable. One way to avoid this problem is to introduce a regularizing IR brane which makes the extra dimension compact, then the continuum becomes discrete KK modes [12] and we can perform calculations just as in the particle case. The continuum limit is obtained by taking the position of the IR brane to infinity. The physical results should not depend on this position, as long as it is much larger than the length scale of the inverse mass gap so that the KK modes are dense enough to approximate a continuum. Even in this case, one may worry about whether the usual narrow-width approximation of splitting a decay chain into steps with independent decays is a good one, as there are an infinite number of KK modes which can make virtual ("off-shell") contributions, reflecting the fact that the continuum state do not have a mass shell to be on. We will discuss the validity of this

approach and compare full calculations with the narrow-width approximation.

This paper is organized as follows. We first review the 5D construction of continuum superpartners, then plough into the details of the decay chains, showing that the narrow-width approximation is generally valid in perturbative theories. We then discuss the phenomenology and the parametric dependence of the observable quantities and give conclusions. A detailed check of the IR regulator is included in the Appendix.

2 A Review of Continuum Superpartners

Let us recall the setup used in Ref. [1], which will be the starting point of our collider studies. We consider a 4D SUSY theory with approximate conformal symmetry. Through the AdS/CFT correspondence [6] this can be modeled by a 5D AdS space. We take the metric of the AdS_5 space to be

$$ds^2 = \left(\frac{R}{z}\right)^2 \left(\eta_{\mu\nu} dx^\mu dx^\nu - dz^2\right) . \tag{1}$$

The space is cutoff at $z = z_{UV} = \epsilon$ by a UV brane where SUSY is broken. As is well known, such a theory can be described in the language of 4D $\mathcal{N} = 2$ superfields, which implies that for each matter field its 5D $\mathcal{N} = 1$ hypermultiplet Ψ can be decomposed into two 4D $\mathcal{N} = 1$ chiral superfields $\Phi = \{\phi, \chi, F\}$ and $\Phi_c = \{\phi_c, \psi, F_c\}$, with the fermionic Weyl components forming a Dirac fermion [13]. In the case of gauge fields, a 5D $\mathcal{N} = 1$ vector superfield can be decomposed into an $\mathcal{N} = 1$ 4D vector superfield $V = \{A_\mu, \lambda_1, D\}$ and a 4D $\mathcal{N} = 1$ chiral superfield $\sigma = \{(\Sigma + iA_5)/\sqrt{2}, \lambda_2, F_\sigma\}$.

As in the usual case of extra-dimensional theories, one can decompose the matter fields as:

$$\chi(p,z) = \chi_4(p) \left(\frac{z}{z_{UV}}\right)^2 f_L(p,z), \qquad \phi(p,z) = \phi_4(p) \left(\frac{z}{z_{UV}}\right)^{3/2} f_L(p,z), \tag{2}$$

$$\psi(p,z) = \psi_4(p) \left(\frac{z}{z_{UV}}\right)^2 f_R(p,z), \qquad \phi_c(p,z) = \phi_{c4}(p) \left(\frac{z}{z_{UV}}\right)^{3/2} f_R(p,z), \tag{3}$$

where the relationships between scalar and fermion profiles are provided by SUSY.

With a fermion bulk mass $m(z) = c + \mu_f z$, the bulk equations of motion give

$$\frac{\partial^2}{\partial z^2} f_R + \left(p^2 - \mu_f^2 - 2\frac{\mu_f c}{z} - \frac{c(c-1)}{z^2} \right) f_R = 0, \tag{4}$$

$$\frac{\partial^2}{\partial z^2} f_L + \left(p^2 - \mu_f^2 - 2\frac{\mu_f c}{z} - \frac{c(c+1)}{z^2} \right) f_L = 0. \tag{5}$$

The solutions for $f_L(p,z)$ and $f_R(p,z)$ can then be expressed as linear combinations of the first order and second order Whittaker functions:

$$f_L(p,z) = a\, M(\kappa, \frac{1}{2}+c, 2\sqrt{\mu_f^2 - p^2}z) + b\, W(\kappa, \frac{1}{2}+c, 2\sqrt{\mu_f^2 - p^2}z) \ , \tag{6}$$

$$\begin{aligned} f_R(p,z) &= -a\, \frac{2(1+2c)\sqrt{\mu_f^2 - p^2}}{p} M(\kappa, -\frac{1}{2}+c, 2\sqrt{\mu_f^2 - p^2}z) \\ &\quad - b\, \frac{p}{(\mu_f + \sqrt{\mu_f^2 - p^2})} W(\kappa, -\frac{1}{2}+c, 2\sqrt{\mu_f^2 - p^2}z) \ , \end{aligned} \tag{7}$$

$$\kappa \equiv -\frac{c\,\mu_f}{\sqrt{\mu_f^2 - p^2}} \ , \tag{8}$$

where a and b are coefficients which may depend on four-momenta p and that are determined by boundary and normalization conditions. We will take all SM fields as left-handed, so we demand that the right-handed chiral superfield $\Phi_c(p,z)$ satisfies the Dirichlet boundary condition at $z = z_{UV}$, *i.e.*, $\Phi_c(p, z_{UV}) = 0$. The left-handed chiral superfield Φ, through the equations of motion, satisfies modified Neumann boundary conditions. As a result, only the left-handed chiral superfield has a normalizable zero-mode. As shown in Ref. [1], the zero mode profile for the left-handed field is given by

$$f_L^0(p,z) = \mathcal{N}(\mu_f, 0) z^{-c} e^{-\mu_f z}, \tag{9}$$

where the normalization factor $\mathcal{N}(\mu_f, 0)$ is obtained from $\int_0^\infty f(0,z) f(0,z)^* dz = 1$,

$$\mathcal{N}(\mu_f, 0) = (2^{-1+2c} \mu_f^{-1+2c}\, \Gamma(1-2c))^{-1/2} \ . \tag{10}$$

In Fig. 1, we show the zero mode profiles for two values of c. As can be seen, when c is positive, the zero mode is localized near the UV brane, while for $c < 0$, the zero mode is repelled away from the UV brane.

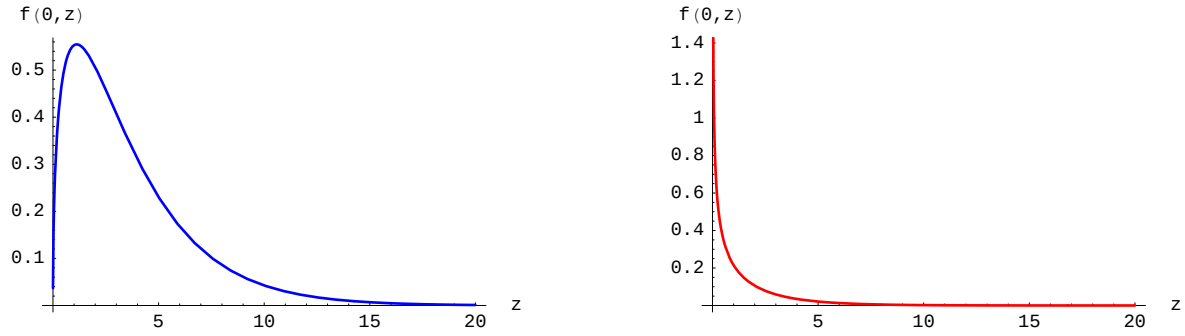

Figure 1: Normalized zero mode profiles. In the left panel we take $c = -0.45$, $\mu_f = 0.4$ TeV while in the right panel, we take $c = 0.45$, and $\mu_f = 0.4$ TeV.

Similarly for gauge fields [1] we write:

$$\lambda_1(p,z) = \chi_4(p) e^{uz} \left(\frac{z}{z_{UV}}\right)^2 h_L, \quad A_\mu(p,z) = A_{\mu 4}(p) e^{uz} \left(\frac{z}{z_{UV}}\right)^{1/2} h_L, \tag{11}$$

$$\lambda_2(p,z) = \psi_4(p) e^{uz} \left(\frac{z}{z_{UV}}\right)^2 h_R, \quad \Sigma = \phi_4(p) e^{uz} \left(\frac{z}{z_{UV}}\right)^{3/2} h_R\,, \tag{12}$$

where $h_{L,R}$ represents $f_{L,R}$ evaluated at $c = 1/2$ and μ_g is related to the dilaton vacuum expectation value [7], $\langle \Phi \rangle = e^{-2\mu_g z}/g_5$.

After including SUSY breaking on the UV brane, the zero mode of the superpartner will be lifted, and the SUSY breaking mass that it acquires depends on the overlap of its wave function with the UV brane. For c close to $+1/2$, the zero mode of the superpartner will acquire a SUSY breaking mass near the full strength (*i.e.*, comparable to the SUSY breaking on the UV brane). On the other hand, if $c < 0$, the SUSY-breaking mass of the zero mode superpartner is suppressed relative to the SUSY breaking on the UV brane. Because $c = 1/2$ for the gauge field, we will take all SM fields to have c close to $1/2$ in this paper in order to have similar SUSY-breaking masses.

The spectrum of nonzero-modes is continuous without an IR cutoff. As mentioned in the Introduction, it is convenient to introduce a regulating IR brane at a large distance $z = z_{IR} = L$ so that we can deal with discrete normalizable KK states [12]. The continuum limit is obtained by taking $L \to +\infty$. The coefficients a and b of the wave functions in Eq. (6-7) can be obtained by imposing the boundary condition on

the IR brane and the normalization condition,

$$\tilde{f}_L(p,z) = \mathcal{N}_L(\mu_f,p)\left(M(\kappa,\frac{1}{2}+c,2\sqrt{\mu_f^2-p^2}z) + b\cdot W(\kappa,\frac{1}{2}+c,2\sqrt{\mu_f^2-p^2}z)\right), \quad (13)$$

$$\tilde{f}_R(p,z) = \mathcal{N}_R(\mu_f,p)\left(\frac{2(1+2c)\sqrt{\mu_f^2-p^2}}{\mu_f-\sqrt{\mu_f^2-p^2}}\cdot M(\kappa,-\frac{1}{2}+c,2\sqrt{\mu_f^2-p^2}z)\right. \quad (14)$$

$$\left. + b\cdot W(\kappa,-\frac{1}{2}+c,2\sqrt{\mu_f^2-p^2}z)\right)\ . \quad (15)$$

Imposing the boundary condition $f_R(p,z_{UV})=0$ we determine that,

$$b = -\frac{M(\kappa,-\frac{1}{2}+c,2\sqrt{\mu_f^2-p^2}z_{UV})}{W(\kappa,-\frac{1}{2}+c,2\sqrt{\mu_f^2-p^2}z_{UV})}\cdot\frac{2(1+2c)\sqrt{\mu_f^2-p^2}}{\mu_f-\sqrt{\mu_f^2-p^2}}\ , \quad (16)$$

and $\kappa\equiv -c\mu_f/\sqrt{\mu_f^2-p^2}$.

We are especially interested in the behavior of the superpartners in the conformal limit at high energies. In the limit of $p\gg\mu_f$, the normalization factor can be expressed as

$$\mathcal{N}_L=-\mathcal{N}_R=\left(\frac{2^{3+4c}\pi\sec^2(c\pi)}{\Gamma(-\frac{1}{2}-c)^2}\cdot z_{IR}\right)^{-1/2}. \quad (17)$$

The gluino profiles can be found similarly by making the replacements $c\to 1/2$ and $\mu_f\to\mu_g$ in Eqs. (13–16).

The KK spectrum is determined by the boundary condition at the IR brane, $f_R(p,z_{IR})=0$, which leads to:

$$\frac{M(-\frac{\mu_g}{2\sqrt{\mu_g^2-p^2}},0,2\sqrt{\mu_g^2-p^2}\ z_{UV})}{W(-\frac{\mu_g}{2\sqrt{\mu_g^2-p^2}},0,2\sqrt{\mu_g^2-p^2}\ z_{UV})}=\frac{M(-\frac{\mu_g}{2\sqrt{\mu_g^2-p^2}},0,2\sqrt{\mu_g^2-p^2}\ z_{IR})}{W(-\frac{\mu_g}{2\sqrt{\mu_g^2-p^2}},0,2\sqrt{\mu_g^2-p^2}\ z_{IR})}. \quad (18)$$

In the limits of interest, $\mu_f,\mu_g\ll p\ll 1/z_{UV}$, the left-hand-side of Eq.(18) tends to zero, which implies that the numerator of the right-hand-side of Eq.(18) satisfies:

$$M(-\frac{\mu_g}{2\sqrt{\mu_g^2-p^2}},0,2\sqrt{\mu_g^2-p^2}\ z_{IR})\propto\cos(\frac{1}{4}\pi-\sqrt{p^2-\mu_g^2}z_{IR})=0. \quad (19)$$

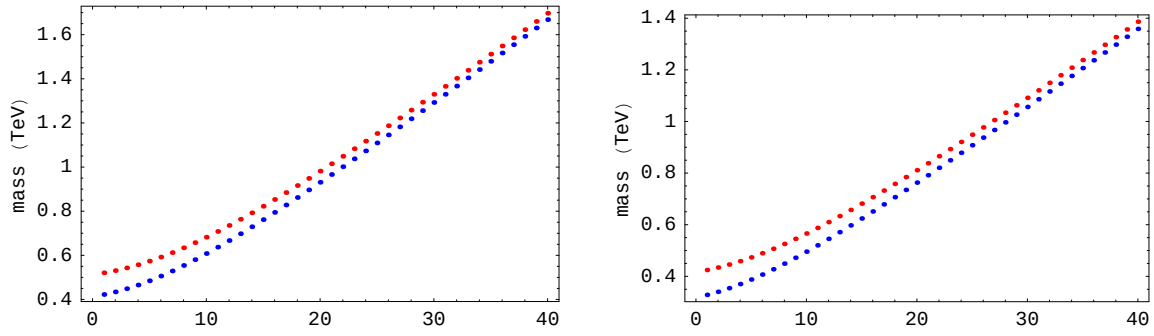

Figure 2: Spectra for the gluino (blue dots) and the squark (red dots). The plot shows mass versus KK mode number. The parameters are chosen to be $z_{UV} = 10^{-3}$ TeV^{-1}, $z_{IR} = 80$ TeV^{-1}, $c = 0.5$, $\mu_g = 0.4$ TeV and $\mu_f = 0.5$ TeV for the left panel, and $z_{UV} = 10^{-3}$ TeV^{-1}, $z_{IR} = 100$ TeV^{-1}, $c = 0.5$, $\mu_g = 0.3$ TeV and $\mu_f = 0.4$ TeV for the right panel.

Solving Eq. (19), we obtain an approximate expression for the KK masses,

$$m_n^2 \approx \mu_g^2 + (\frac{1}{4} + n)^2 \pi^2 / z_{IR}^2 \qquad \text{with} \qquad n = 0, 1, 2, \cdots . \tag{20}$$

Some sample spectra are shown in Fig. 2, where we have taken $z_{UV} = R = 10^{-3}$ TeV^{-1} and $c = 1/2$. With mass gaps on the order of half a TeV, a 20 GeV mode spacing is quite a good approximation to a continuum.

3 Continuum Decay Chains and Narrow-Width Approximations

Now we would like to study the decay of a continuum superpartner. The question is: what are the characteristic features of the decay process? Does it prefer to decay through multiple steps and emit soft particles during the decays, or to decay directly down to the bottom of the spectrum together with a hard particle? What is the typical energy of the visible particles produced in the decay chain relative to the energy and other parameters of the superpartner? As mentioned earlier, in order to use the calculation techniques developed for particles, it is convenient to include a regularizing IR

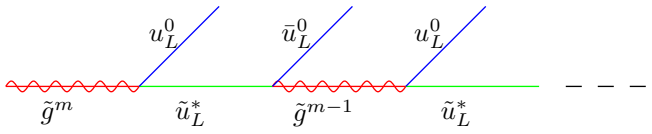

Figure 3: Feynman diagram for sequential KK gluino decay.

brane to discretize the continuum into KK modes [12], so that we can deal with ordinary particles in the initial and final states. To study the validity of the narrow-width approximation of the decay chain, which splits the process into a sequence of independent decays at each step, we compare the result from a calculation of a sequence of real two 2-body decays with that of the 3-body decay which includes all the contributions from the virtual intermediate continuum superpartner. We assume that we start with an initial state with an invariant mass much higher than the mass gaps and the SUSY breaking mass. To simplify the calculations, we will ignore the SUSY-breaking and the masses of the SM particles. We find that, in the case that the calculations are reliable (*i.e.*, independent of $z_{IR} = L$ as long as $L \gg p^{-1}, \mu_f^{-1}, \mu_g^{-1}$), the virtual contributions are indeed smaller than the real contributions so that the narrow-width approximation is reliable.

3.1 The 2-body gluino decay calculation

Once we include a regulating IR brane to make the spectra discrete, the calculation of a 2-body decay should be straightforward. We consider an initial state of a gluino of KK level m, decaying in its rest frame to a quark and a KK squark of level n, $\tilde{g}^m \to u_L^0 \tilde{u}_L^{*,n}$. Since we ignore the quark mass, the decay can occur to any KK squark lighter than the initial gluino. The energy of the emitted quark depends on which level of the KK squark the gluino decays to. To calculate the decay rate, we need the coupling between the gluino, squark, and the quark. The effective interaction of the KK gluino, KK

squark and the quark in momentum space is given by:

$$S_{eff} = c(p_m, q_n) \int \frac{d^4p_n}{(2\pi)^4} \frac{d^4q_m}{(2\pi)^4} \; u_L^0(p_m - q_n) \; \tilde{u}_L^{m,*}(q_n) \; \tilde{g}^n(p_m) \; , \tag{21}$$

where $c(p_m, q_n)$ is the vertex coefficient which can be computed by integration of the gluino, squark and quark 5D profiles over the fifth dimension. The expression is:

$$\begin{aligned} c(p_m, q_n) \;\; = \;\; & \mathcal{N}_{\tilde{g}}(\mu_g, p_m) \; \mathcal{N}_{\tilde{u}}(\mu_f, q_n)^* \; \mathcal{N}_u(\mu_f, 0) \; g_5 \int_{z_{UV}}^{z_{IR}} dz \left(\frac{z_{UV}}{z}\right)^5 \;\; \left(\frac{z}{z_{UV}}\right)^2 e^{-\mu_f z} z^{-c} \\ & \left(\frac{z}{z_{UV}}\right)^{3/2} f_L(q_n, z)^* \; e^{uz} \left(\frac{z}{z_{UV}}\right)^2 h_L(p_m, z) \; , \end{aligned} \tag{22}$$

where g_5 is the 5D gauge coupling, which only enters the calculation as an overall factor. The 4D gauge coupling g_4 is related to the 5D gauge coupling g_5 by integrating over the zero mode profiles in the kinetic term for the gauge fields coupled with the dilaton. In that case one finds [7] that,

$$g_4^2 = \frac{g_5^2}{z_{UV}} \frac{1}{\log(1/(2 z_{UV} \mu_g)) - \gamma_E)}, \tag{23}$$

where γ_E is Euler's constant. Since we are interested in the gluino decay into a quark and a squark, we consider the QCD gauge coupling which equals $\alpha_s(m_Z) = 0.1184$ at the Z-mass. If we take $z_{UV} = 10^{-3}$ TeV^{-1} and the nominal value for the gluino mass gap of $\mu_g = 0.1$ TeV,[2] the 5D strong gauge coupling assumes the dimensionful value $g_5 = 0.108$ TeV$^{-1/2}$.

An immediate observation from Eq. (22) is that a finite coupling in the limit $z_{IR} \to +\infty$ is obtained only for $\mu_f > \mu_g$. For $\mu_f < \mu_g$, the integral is dominated by the large z region and it blows up as we take $z_{IR} \to +\infty$. In this case we cannot perform a sensible calculation. One can see that the exponentially growing factor comes from the dilaton profile for the KK gluino, which is a result of that the zero mode gauge field has to be a constant along the fifth dimension due to gauge invariance. A similar situation happens in the Randall-Sundrum 2 (RS2) scenario [14]. If one calculates the self interactions among KK gravitons in RS2 with a regulating IR brane, one also

[2]The dependence on the gluino mass gap μ_g is only logarithmic, reflecting the gauge coupling's running.

finds that the coupling blows up as one takes the IR brane to infinity. In the 4D CFT picture, these KK gravitons correspond to the conformal bound states. The large coupling just means that these bound states are strongly coupled. These divergent couplings can never make any physical process involving UV zero-modes infinite. As is well known, the KK picture sometimes can give misleading results when locality in the extra dimension is involved. The point is that any process starting with zero-modes localized on the UV brane will mostly be sensitive to the physics near the UV brane due to the locality in the extra dimension. The "nonlocal" process of producing KK gravitons in the deep IR region must be suppressed due to interference of various diagrams even though each of them can have a large coupling. In our theory, all zero-modes are localized near the UV brane (for $c \sim 1/2$), so all physical processes originated from the zero-modes should also only be sensitive to the physics near the UV brane. The divergent coupling in the $\mu_f < \mu_g$ case just means that the naïve calculations done in the KK picture are not valid. On the other hand, for $\mu_f > \mu_g$ the integral is dominated by the region near the UV brane, and the calculations are trustworthy. For the same reason, the coupling between a KK gluino, a KK squark, and a KK quark is also dominated by the IR region and diverges when the IR brane is moved to infinity. However, since the wave functions of the KK quarks are suppressed in the UV region, the decay to a KK squark plus a KK quark should also be suppressed if the initial KK gluino was produced in the UV region in the first place. To avoid such complications, we will restrict our study to the $\mu_f > \mu_g$ case and consider decays to the quark zero mode only in this paper.

After obtaining the coupling, it is straightforward to calculate the decay rate to each KK squark. To compare with the continuum limit, we express the result in terms of the differential decay rate as a function of the energy of the outgoing quark:

$$\begin{aligned} \frac{d\Gamma_{\tilde{g}^m \to u_L^0 \tilde{u}_L^{n,*}}}{dE_{u_L^0}} &\approx \sum_{n \in\, \mu_f < E_n < E_m} \frac{\Delta\Gamma_{\tilde{g}^m \to u_L^0 \tilde{u}_L^{n,*}}}{\Delta E_{u_L^0}} \\ &\approx \sum_{n \in\, \mu_f < E_n < E_m} \frac{c(p_m, q_n) c^\dagger(p_m, q_n)}{\Delta E_{u_L^0}} \frac{E_{u_L^0}^2}{4\pi p_m} \frac{\mathrm{Tr}[t^a t^a]}{8} \end{aligned} \tag{24}$$

where t^a are the SU(3) generators in the fundamental representation and $p_m \equiv \sqrt{p_m^2}$.

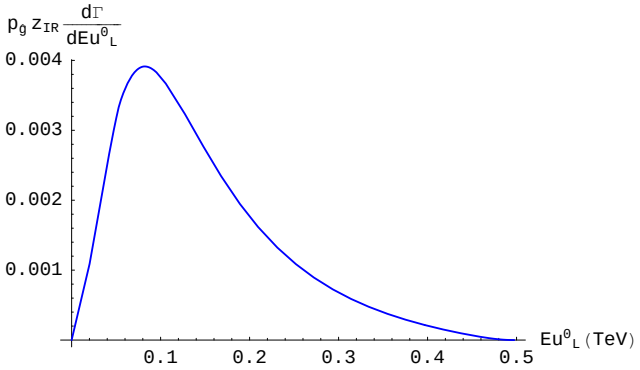

Figure 4: Gluino differential decay rate with respect to the first quark energy. The initial KK gluino mass is $p_{\tilde{g}} = 1.15$ TeV and we use $g_5 = 0.108$ TeV$^{-1/2}$. We choose $z_{UV} = 10^{-3}$ TeV^{-1}, $z_{IR} = 100$ TeV^{-1}, $c = 0.5$, $\mu_g = 0.3$ TeV and $\mu_f = 0.4$ TeV.

From conservation of energy-momentum we have,

$$E_{u_L^0} = \frac{1}{2} p_m \left(1 - \frac{q_n^2}{p_m^2}\right), \tag{25}$$

which implies

$$\Delta E_{u_L^0} = \frac{1}{2} p_m \left(1 - \frac{q_{n-1}^2}{p_m^2}\right) - \frac{1}{2} p_m \left(1 - \frac{q_n^2}{p_m^2}\right) . \tag{26}$$

A typical differential decay rate as a function of the outgoing quark energy is shown in Fig. 4. We have normalized the decay rate by a factor $p \cdot z_{IR}$ as we do with all differential decay rate figures hereafter, in order to cancel the unphysical IR dependence $\Delta m_n = \pi / z_{IR}$ in the continuum limit.[3] At small quark energies, the decay rate is suppressed by phase space, while at large quark energies, the decay rate is suppressed by the couplings due to the small overlap between the gluino and squark wave functions of large KK level differences. Overall we see that the suppression due to the coupling

[3]It is easy to see that the coupling is proportional to L from the normalizations of the gluino and squark wave functions. The differential decay rate of a single KK gluino is proportional to $(1/L)^2 \times L = 1/L$ as the density of the final KK squarks is proportional to L. This is related to the fact that the overlap of a single KK gluino wave function with the UV region where the zero modes are located is also proportional to $1/L$. In reality the initial KK gluino will be produced with some energy range and the number of KK gluinos in that energy range is again proportional to L, which cancels the unphysical $1/L$ dependence in the differential decay rate of a single KK mode.

is stronger and the outgoing quark has a relatively soft spectrum. The suppression of high energy emissions is exactly the behavior that is expected in a CFT [8–11]. Starting with very high KK modes this leads to approximately spherical events [11]. A more detailed discussion of the quark spectrum and its parameter dependence will be presented in the next section after the narrow-width approximation is justified.

3.2 The 5D mixed position-momentum propagator

From the previous subsection we see that the result of the 2-body calculation shows that the gluino prefers to decay to the squark with a mass not far below the gluino mass. This means that the resulting squark is likely to decay again back to the gluino and the whole process will involve a long decay chain. An important question is whether the sequence of decays can be treated independently and correlations implied by the full intermediate propagator can be safely neglected. This question is less trivial for the continuum case than the usual particle case because there are an infinite number, a continuum, of intermediate states which can give contributions at each step. To study this problem, we consider the 3-body gluino decay process $\tilde{g}^m \to u_L^0 u_L^{0*} \tilde{g}^n$ where the continuum squark is in the intermediate state. We will calculate the contribution from the virtual ("off-shell") intermediate squark while using real KK modes for the initial and final states.

In the KK picture with a regulating IR brane, the intermediate squark propagator is simply a sum of the particle propagators of all KK levels [12]. The propagator of an individual scalar particle is

$$\lim_{\epsilon \to 0^+} \frac{i}{q^2 - m_n^2 + i\epsilon} = \pi \delta(q^2 - m_n^2) + i\,\mathcal{P}\frac{1}{q^2 - m_n^2} \tag{27}$$

where $\mathcal{P}$ denotes the Cauchy principal value. The delta function (the real part) represents the phase space for a real intermediate particle (the "on-shell" contribution), while the second term (the imaginary part) represents the contribution of a virtual intermediate state (the "off-shell" contribution). However, the KK picture is not the most convenient one to perform calculations with virtual intermediate states as it involves an infinite sum of singular functions. We know that in the continuum limit,

the infinite sum of KK propagators simply becomes the unparticle propagator [12], and the series of poles on the positive real axis of p^2 merge into a branch cut of the unparticle propagator. Therefore, we will employ the full unparticle propagator for the intermediate state in our calculation. In this subsection we derive the unparticle propagator in mixed position-momentum space [15].

The left-handed scalar propagator satisfies the equation of motion for the left-handed profile, with a delta-function source,

$$\left(-\partial_z^2 + \frac{3}{z}\partial_z + (c^2 + c - \frac{15}{4})\frac{1}{z^2} + \frac{2c\mu_f}{z} + \mu_f^2 - p^2\right) iP(p,z,z') = \left(\frac{z}{z_{UV}}\right)^3 \delta(z-z'), \quad (28)$$

and the UV boundary condition for the propagator is

$$\left(\partial_z + \frac{1}{z}(-\frac{3}{2} + c + \mu_f z)\right) P(p,z,z')\Big|_{z=z_{UV}} = 0. \quad (29)$$

To connect to the continuum limit, with outgoing boundary conditions, we demand that the propagator is exponentially damped [15] at large Euclidean momenta:

$$P(ip, z_{IR}, z')|_{p\to+\infty, z'<z_{IR}} \to e^{-p\, z_{IR}}. \quad (30)$$

In order to solve Eq. (28–29) for $P(p,z,z')$, we look for solutions in the regions $z > z'$, $P_>(p,z,z')$, and $z < z'$, $P_<(p,z,z')$, and use matching boundary conditions at $z = z'$,

$$P_<(p,z,z') - P_>(p,z,z')|_{z=z'} = 0, \quad (31)$$

$$\partial_z P_<(p,z,z') - \partial_z P_>(p,z,z')|_{z=z'} = -i\left(\frac{z}{z_{UV}}\right)^3. \quad (32)$$

We can write the general solution to Eq. (28) in terms of two independent solutions to the homogeneous equation [15], $K(p,z)$ and $S(p,z)$:

$$K(p,z) = \left(\frac{z}{z_{UV}}\right)^{3/2} \frac{W(\kappa, \frac{1}{2}+c, 2\sqrt{\mu_f^2 - p^2}z)}{W(\kappa, \frac{1}{2}+c, 2\sqrt{\mu_f^2 - p^2}z_{UV})}, \quad (33)$$

$$\begin{aligned} S(p,z) = {} & \left(\frac{z}{z_{UV}}\right)^{3/2} \frac{1}{2\sqrt{\mu_f^2 - p^2}} \frac{\Gamma(1+c-\kappa)}{\Gamma(2+2c)} \\ & \left(M(\kappa, \frac{1}{2}+c, 2\sqrt{\mu_f^2 - p^2}z)\; W(\kappa, \frac{1}{2}+c, 2\sqrt{\mu_f^2 - p^2}z_{UV})\right. \\ & \left. -W(\kappa, \frac{1}{2}+c, 2\sqrt{\mu_f^2 - p^2}z)\; M(\kappa, \frac{1}{2}+c, 2\sqrt{\mu_f^2 - p^2}z_{UV})\right), \end{aligned} \quad (34)$$

which satisfy the following boundary conditions:

$$K(p, z_{UV}) = 1, \qquad K(ip, z)|_{p\to+\infty} \to e^{-pz}, \qquad S(p, z_{UV}) = 0, \qquad S'(p, z_{UV}) = 1. \quad (35)$$

In the region $z < z'(z > z')$, the general solution can be written as

$$P_{<(>)}(p, z, z') \;\; = \;\; a_{<(>)}\; K(p, z) + b_{<(>)}\; S(p, z). \quad (36)$$

The boundary condition at the UV brane, Eq. (29), fixes the ratio of $a_</b_<$ to be proportional to the kinetic function $\Sigma_{F_c}(p)$ already encountered in Ref. [1]:

$$\frac{a_<}{b_<} = \frac{\Sigma_{F_c}(p)}{z_{UV}} = \frac{(\mu_f + \sqrt{\mu_f^2 - p^2})}{p^2} \frac{W\left(-\frac{c\mu_f}{\sqrt{-p^2+\mu_f^2}}, \frac{1}{2} + c, 2\sqrt{-p^2+\mu_f^2}\; z_{UV}\right)}{W\left(-\frac{c\mu_f}{\sqrt{-p^2+\mu_f^2}}, \frac{1}{2} - c, 2\sqrt{-p^2+\mu_f^2}\; z_{UV}\right)}\,, \quad (37)$$

$$\Sigma_{F_c}(p) \;\; = \;\; z_{UV} \cdot \left(\frac{R}{z_{UV}}\right)^3 \frac{1}{p} \frac{f_L}{f_R}\,. \quad (38)$$

The kinetic function $\Sigma_{F_c}(p)$ not only fixes the spectral density, but it is also essential in determining the phase space. Using the required IR behavior of $P(p, z, z')$, we conclude that $P_>(p, z, z')$ can only be proportional to $K(p, z)$, (*i.e.*, $b_> = 0$). At this stage we use the matching conditions at $z = z'$, so that in the range $z < z'$, the left-handed squark propagator can be expressed as [15]:

$$i\, P(p, z, z') \;\; = \;\; \frac{\Sigma_{F_c}(p)}{z_{UV}} K(p, z)K(p, z') - S(p, z)K(p, z')\,. \quad (39)$$

For the case $z > z'$ we just interchange $z \leftrightarrow z'$ in Eq. (39).

Obviously for $p^2 > \mu_f^2$, $\sqrt{\mu_f^2 - p^2}$ becomes imaginary, so the propagator has a branch cut on the real axis for $p^2 > \mu_f^2$, and the discontinuity is just twice the real part. This discontinuity corresponds to a real intermediate unparticle (the "on-shell" contribution). From the analogy of the particle propagator (27) we interpret the imaginary part of the unparticle propagator as the virtual ("off-shell") contribution to the 3-body decay process, while the real part (the discontinuity) corresponds to the phase space of the unparticle. In fact, one can use this phase space to calculate directly the real 2-body differential decay rate considered in the previous subsection, instead

of summing over KK modes in a discretized theory. In the Appendix we show the equivalence of the two pictures in the limit that the IR regulator is removed, $L \to \infty$. The numerical results for the 2-body differential decay rates using the two approaches also agree well for large L.

3.3 The 3-body gluino decay

With the unparticle propagator derived in the previous subsection, we can compute the virtual contribution to the 3-body decay process, $\tilde{g}^m \to u_L^0 u_L^{0*} \tilde{g}^n$. We take both the initial and final gluinos to be KK states in an IR regularized theory, but use the unparticle propagator for the intermediate state with only the imaginary part corresponding to the virtual contribution. It is straightforward to find the amplitude squared for the virtual 3-body process by integrating the imaginary part of the propagator $P(q, z, z')$ derived in Eq.(39) over the positions of the two vertices in the extra dimension,

$$\left|M(\tilde{g}^m \to u_L^0 u_L^{0*} \tilde{g}^n)\right|^2 = 4 g_5^4 \ |v(p_{\tilde{g}^m}, q, p_{\tilde{g}^n})|^2 \ (p_{\tilde{g}^m}.p_{u_L^{0*}}) \ (p_{u_L^0}.p_{\tilde{g}^n}) \ . \tag{40}$$

We have labeled the 4-momenta of the initial, final, and intermediate states as follows: $p_{\tilde{g}^m}$ for the initial gluino $\tilde{g}^m$, $p_{\tilde{g}^n}$ for the outgoing gluino $\tilde{g}^n$, $p_{u_L^0}$ for the quark, $p_{u_L^{0*}}$ for the anti-quark, and q for the intermediate squark. The factor $v(p_m, q, p_n)$ is given by the integration in the extra dimension of the respective profiles and the propagator:

$$\begin{aligned} v(p_{\tilde{g}}^n, q, p_{\tilde{g}}^m) \ &= \ \mathcal{N}_u^2(\mu_f, 0) \mathcal{N}_{\tilde{g}}(\mu_g, p_{\tilde{g}}^m) \mathcal{N}_{\tilde{g}}(\mu_g, p_{\tilde{g}}^n) \\ &\quad \times \int_{z_{UV}}^{z_{IR}} dz \int_{z_{UV}}^{z_{IR}} dz' \ e^{(\mu_g - \mu_f) z} z^{1/2-c} h_L(p_{\tilde{g}}^m, z) z_{UV}^{-1} \tilde{P}(q, z, z') \\ &\qquad\qquad e^{(\mu_g - \mu_f) z'} z'^{1/2-c} h_L(p_{\tilde{g}}^n, z') \ , \end{aligned} \tag{41}$$

here we use a rescaled scalar propagator, $\tilde{P}(q, z, z') = \left(\frac{z}{z_{UV}}\right)^{-3/2} \left(\frac{z'}{z_{UV}}\right)^{-3/2} P(q, z, z')$, and we can write the differential decay rate as:

$$\frac{d\Gamma_3}{dE_u} = g_5^4 \ v(p_{\tilde{g}}^m, q, p_{\tilde{g}}^n) v(p_{\tilde{g}}^m, q, k_{\tilde{g}}^n)^\dagger \ \frac{E_u^2 (2 E_u p_{\tilde{g}}^m - (p_{\tilde{g}}^m)^2 + (p_{\tilde{g}}^n)^2)^2}{32 p_{\tilde{g}}^m (2E_u - p_{\tilde{g}}^m) \pi^3} \frac{1}{8} \mathrm{Tr}[t^a t^b t^b t^a] \tag{42}$$

where $E_{u_L^0}$ is the energy of the (first) outgoing quark in the initial gluino rest frame and $\frac{1}{8}\mathrm{Tr}[t^a t^b t^b t^a] = \frac{1}{8} C_A C_F^2 = 2/3$ for $SU(3)$. The range of $E_{u_L^0}$ is determined by the

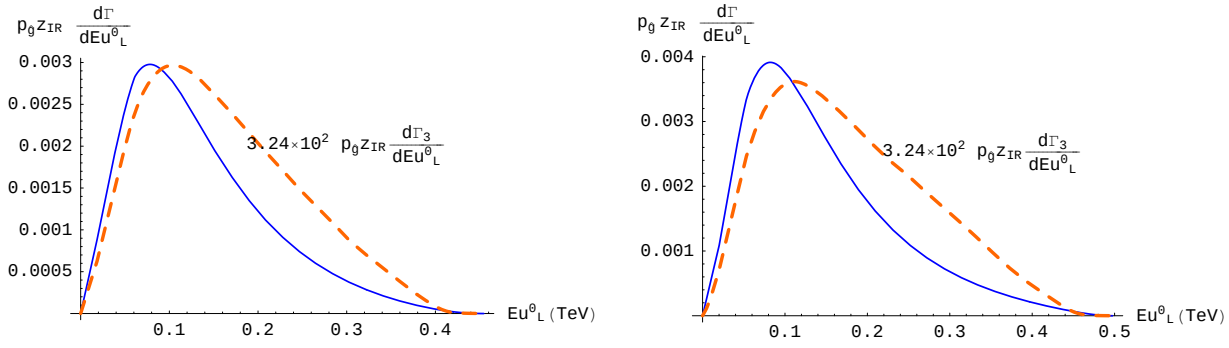

Figure 5: Gluino decay rate with respect to the first quark energy. The yellow dash line represents the virtual contribution from three body decay which is rescaled by a factor of 3.24×10^2 , while the blue line represents two body decay result. In both plots, the initial KK gluino mass is $p_{\tilde{g}} = 1.15$ TeV and we use $g_5 = 0.108$ TeV$^{-1/2}$. In the left one, we choose $z_{UV} = 10^{-3}$ TeV^{-1}, $z_{IR} = 80$ TeV^{-1}, $c = 0.5$, $\mu_g = 0.4$ TeV and $\mu_f = 0.5$ TeV; In the right one, we choose $z_{UV} = 10^{-3}$ TeV^{-1}, $z_{IR} = 100$ TeV^{-1}, $c = 0.5$, $\mu_g = 0.3$ TeV and $\mu_f = 0.4$ TeV.

masses of the initial and final gluinos:

$$E_{u_L^0\,\min} = 0\,, \tag{43}$$

$$E_{u_L^0\,\max} = \frac{1}{2}\, p_{\tilde{g}}^m \left(1 - \frac{(p_{\tilde{g}}^n)^2}{(p_{\tilde{g}}^m)^2}\right)\,. \tag{44}$$

The contribution to the differential decay rate as a function of the outgoing quark energy from the virtual 3-body process can be compared with the real 2-body contribution by summing over all final KK gluinos and outgoing anti-quark energies which are kinematically allowed. The result is shown in Fig. 5. The virtual 3-body process is the cut of a two-loop diagram while the real 2-body process is the cut of a one-loop diagram, so we expect that the 3-body decay rate should be suppressed with respect to the 2-body decay rate by a 4D loop factor as long as the theory remains perturbative. The shapes of the two contributions are also similar, but with the 3-body contribution being slightly harder. Thus we can conclude that in this case, it is reasonable to use the narrow-width approximation to calculate the energy distributions of the visible

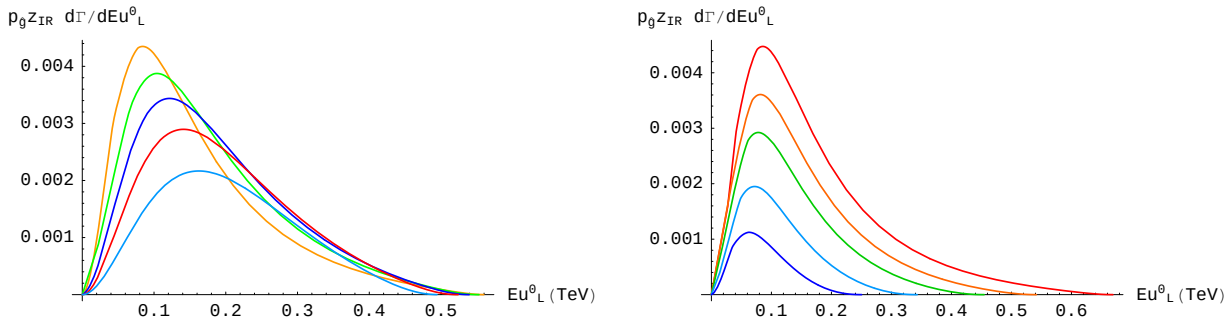

Figure 6: 2-body gluino differential decay rate as a function of the outgoing quark energy $E_{u_L^0}$ in TeV. We have taken in this example $z_{UV} = 10^{-3}$ TeV^{-1}, $z_{IR} = 80$ TeV^{-1}, $c = 1/2$ and $g_5 = 0.108$ TeV$^{-1/2}$. In the figure on the left, we fixed the initial gluino KK-mass at $p_{\tilde{g}} = 1.26$ TeV and its mass-gap to $\mu_g = 0.3$ TeV, and vary the squark mass gap by $\mu_f = 0.40\,, 0.43\,, 0.46\,, 0.50\,, 0.56$ TeV. As can be seen from the figure, the peak position decreases in magnitude and shifts towards larger values of $E_{u_L^0}$. In the figure on the right, we fixed $\mu_g = 0.4$ TeV and $\mu_f = 0.5$ TeV, and vary the initial gluino KK-mass by $p_{\tilde{g}} = 0.83\,, 0.97\,, 1.15\,, 1.29\,, 1.52$ TeV. In this case the peak increases in magnitude with increasing p and its position remains roughly constant as a function of $E_{u_L^0}$.

particles coming from the continuum decays by treating each decay step going to real states that subsequently decay independent of the details of the previous decay.

4 Phenomenology of the Continuum Superpartner Decays

The comparison of the differential decay rate calculations for a real 2-body process and a virtual 3-body process in the previous section, shows that it is reasonable to calculate the energy distributions of the visible particles coming from the continuum superpartner decays using the narrow-width approximation. This greatly simplifies the phenomenological study of continuum superpartners. As mentioned earlier, the contin-

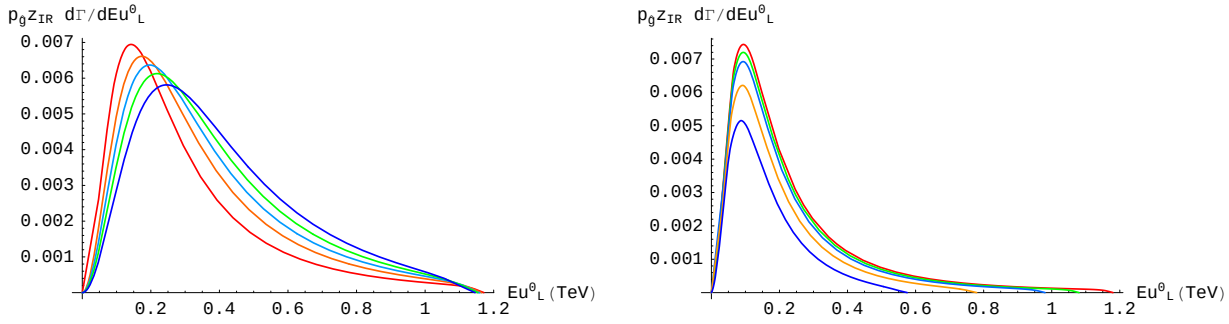

Figure 7: Same as Fig. 6 for different sets of energies and mass gaps. In the plot on the left, we fixed $p_{\tilde{g}} = 2.4$ TeV, and $\mu_g = 0.2$ TeV. We vary the squark mass gap by $\mu_f = 0.36\ , 0.40\ , 0.43\ , 0.46\ , 0.5$ TeV. As can be seen, the peak decreases in magnitude and slightly moves towards larger values of $E_{u_L^0}$. In the figure on the right, we fixed $\mu_g = 0.2$ TeV and $\mu_f = 0.3$ TeV, and vary the initial gluino KK-mass by $p_{\tilde{g}} = 1.24\ , 1.62\ , 2.01\ , 2.21\ , 2.4$ TeV. In this case, the peak magnitude increases and its position remains roughly constant with respect to $E_{u_L^0}$.

uum states tend to decay to other continuum states that are nearby in invariant mass, and so the ordinary particles tend to be emitted with soft energies. This is the behavior that is expected in a CFT [8–11]. Thus if the decay chain starts fairly high up in the continuum, then there is usually a long decay chaining with an approximately spherical distribution of energy [11]. In this section, we examine how the energy distributions of the visible particles depend on the parameters of the theory and the process.

As the energy of the emitted quark $E_{u_L^0}$ increases (or what is the same, the squark mass q_n decreases), the phase space of the final particles increases while the vertex $c(p_n, q_m)$ decreases. It is the competition between these two factors that makes the differential decay rate have its maximum at an quark energy around $E_{u_L^0,\max} \sim (\mu_f - \mu_g)$ as can be seen in Figs. 6 and 7. As a consequence, for a high-energy initial state ($p_{\tilde{g}} \gg \mu_f,\ \mu_g$), we expect order $p_{\tilde{g}}/(\mu_f - \mu_g)$ particles coming out a decay chain. For fixed g_4, c, z_{IR}, and z_{UV}, there are only three parameters: the initial gluino energy $p_{\tilde{g}}$ and the two mass gaps μ_f, μ_g. Since there should be little dependence on z_{IR} and z_{UV}, as long as they are far away from the energy scale interested, physical quantities

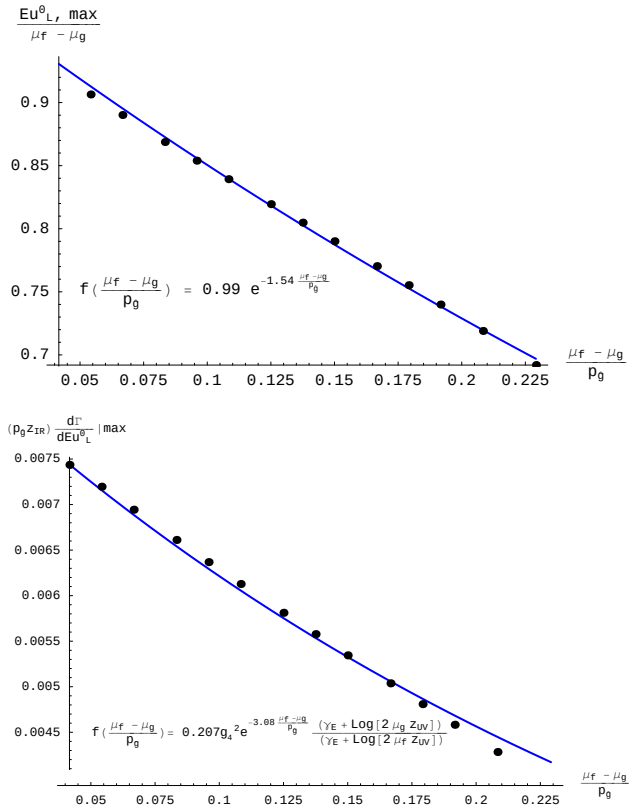

Figure 8: $\frac{E_{u_L^0,max}}{\mu_f-\mu_g}$ vs. $\frac{\mu_f-\mu_g}{p_{\tilde{g}}}$ and $(p_{\tilde{g}} z_{IR})\frac{d\Gamma}{dE_{u_L^0}}|_{max}$ vs. $\frac{\mu_f-\mu_g}{p_{\tilde{g}}}$ evaluated at the peak positions. We use $z_{UV} = 10^{-3}$ TeV^{-1}, $z_{IR} = 80$ TeV^{-1}, $c = 0.5$ and $g_5 = 0.108$ TeV$^{-1/2}$ and fix $p_{\tilde{g}} = 2.40$ TeV, $\mu_g = 0.2$ TeV, while the squark mass gap is varied from $\mu_f = 0.3$ TeV to $\mu_f = 0.75$ TeV. The plots display the fitted functions.

can be expressed as functions of the two dimensionless ratios of $p_{\tilde{g}}$, μ_f, and μ_g up to an overall normalization. In Fig. 8 we show the dependence of the peak position and magnitude of the differential decay rate on the initial energy $p_{\tilde{g}}$ and the mass gap difference $\mu_f - \mu_g$. From these figures we can determine an approximate behavior for the peak position, $E_{u_L^0,\max}$ in the differential decay rate as a function of $\mu_f - \mu_g$ and $p_{\tilde{g}}$. We find that it can be parameterized by an exponential decaying function with an overall normalization A and a numerical exponent B:

$$E_{u_L^0,\max} = A(\mu_f - \mu_g)\; e^{-B\frac{(\mu_f-\mu_g)}{p_{\tilde{g}}}} \quad . \tag{45}$$

The numerical values of A and B are obtained by fitting numerical data points, as shown

in Fig. 8, where we find that $A \approx 1$ and $B \approx 3/2$. Using the plane wave approximation for the wave functions of the incoming gluino and outgoing squark, the coupling squared is proportional to $|c(p_m, q_n)|^2 \propto \frac{1}{z_{IR}^2\ (\mu_f - \mu_g)^2}$. Then one can substitute Eq.(45) into Eq.(24), using $\Delta E_{u_L^0} \approx \pi / z_{IR}$, to obtain an approximate analytical expression for $(d\Gamma / dE_{u_L^0})|_{E_{u_L^0,\max}}$ as a function of μ_f and μ_g:

$$\left(p_{\tilde{g}} z_{IR} \frac{d\Gamma}{dE_{u_L^0}} \right) \Bigg|_{E_{u_L^0,max}} = C \cdot g_4^2 \frac{e^{-2B\frac{(\mu_f - \mu_g)}{p_{\tilde{g}}}}}{4\pi^2} \frac{(\log(1/(2\mu_g z_{UV})) - \gamma)}{(\log(1/(2\mu_f z_{UV})) - \gamma)} \tag{46}$$

the overall normalization C compensates for the inaccuracy of the plane wave approximation, and we have written everything in terms of 4D quantities. The dependence on z_{UV} is only logarithmic and therefore mild. To give an idea of the validity of the approximation, we plot against numerical data in the second plot of Fig. 8. We see that (45) and (46) provide reasonably good estimates for the functional dependence.

5 Conclusions

Supersymmetry is one of the best motivated scenarios for new physics beyond the standard model at the TeV scale. For the past two decades it has been intensively searched for. Currently, the experiments at the LHC have placed very strong limits on the masses of the squarks and gluino to be above ~ 1 TeV in the standard scenario [16–18]. This means that either the superpartner spectrum is unnaturally heavy or the superpartners decay in unusual ways which escape the standard SUSY searches. As we showed in this paper, if the superpartners have continuous spectra, they tend to have long decay chains and produce many soft SM particles. This is a challenging scenario at the LHC because the soft particles may not pass the experimental cuts, and the signals could be buried in the QCD backgrounds. It may require a more specialized study to search for this kind of signal.

Naïvely the phenomenological studies of continuum superpartners at colliders may appear to be formidable as the usual calculation techniques have only been developed

for particles. Here we have seen that these methods can still be used in continuum calculations. In particular, we showed that the narrow-width approximation is still generally valid in the perturbative decay processes that we are interested in. This greatly simplifies the calculations because processes with long sequences of decays can be divided into individual steps involving real states and each step can be calculated independently. The easiest way to perform the calculations is to introduce a regularizing IR brane in the 5D picture which transforms the continuum into discrete KK modes, then one can carry out the calculations as in the usual particle case. As long as the KK modes have reasonably fine spacings, the results are basically independent of the position of the IR brane. In this way, continuum superpartners can also be implemented in the usual collider simulation tools in order for more detailed studies to develop new strategies to search for such kinds of exotic collider signals.

Acknowledgments

We thank Jack Gunion and Markus Luty for useful discussions and comments. We also thank the Aspen Center for Physics and the Kavli Institute for Theoretical Physics where part of this work was completed. The authors were supported by the US Department of Energy under contract DE-FG02-91ER406746.

A Equivalence of the Continuum and KK Limit

It is interesting to compare our expression for the propagator. Eq. (39), with the more familiar KK-representation of the 5D propagator which can be expressed as sum over the different KK-level propagators:

$$P_{KK}(q, z, z') = \sum_n \frac{\tilde{f}_L(m_n, z)\ \tilde{f}_L^\dagger(m_n, z')}{q^2 - m_n^2 - i\ \epsilon}, \tag{47}$$

where $\tilde{f}_L(m_n, z)$ is the normalized left-handed squark wavefunction. This propagator corresponds to a real particle when $q^2 = m_n^2$ (aka going "on-shell") for each particular

KK-mode n. For momenta q close to m_n, we can use the approximation,

$$\frac{i}{q^2 - m_n^2 + i\epsilon} = \pi\delta(q^2 - m_n^2) + i\,\mathcal{P}(\frac{1}{q^2 - m_n^2}), \tag{48}$$

where $\mathcal{P}$ denotes the Cauchy principal value. As the mass difference between adjacent KK-levels n and $m = n-1$ tends to zero (the continuum limit), $\Delta m_n = m_n - m_m \to 0$, the sum over KK-levels in Eq. (47) becomes an integral in the complex plane over "tightly squeezed" resonances which form a branch cut in the limit $z_{IR} \to \infty$. Thus, we can identify the real ("on-shell") contribution of the continuum propagator, Eq. (39), by matching the continuum limit of Eq. (47) with Eq. (39). For that purpose, we consider Eq. (47) in the limit $\mu_f \ll q \ll 1/z_{UV}$. Let us take $z = z' = z_{UV}$ and using Eq. (13) and Eq. (17), in the case $c = 1/2$ for simplicity, we find that:

$$\begin{aligned}\left|\tilde{f}_L(m_n, z_{UV})\right|^2 &\to \left|\mathcal{N}_L\left(-\frac{M(0,0,2im_n z_{UV})}{W(0,0,2im_n z_{UV})}W(0,1,2im_n z_{UV})\right)\right|^2 \\ &\to \frac{\pi}{z_{IR}}\frac{1}{\sqrt{m_n^2}z_{UV}\left(\left(\log\left(\frac{m_n}{2}\right) + \log(z_{UV}) + \gamma_E\right)^2 + \frac{\pi^2}{4}\right)}.\end{aligned} \tag{49}$$

By identifying $\Delta m_n = \pi/z_{IR}$ and using Eq. (48), we find that:

$$\begin{aligned}&\mathrm{Im}[P_{KK}(q, z_{UV}, z_{UV})] \to \sum_n \left|\tilde{f}_L(m_n, z_{UV})\right|^2 \pi\delta(q^2 - m_n^2) \\ \to\ &\frac{\pi/2}{q^2 z_{UV}\left(\left(\log\left(\frac{q}{2}\right) + \log(z_{UV}) + \gamma_E\right)^2 + \frac{\pi^2}{4}\right)} = \mathrm{Im}[\frac{\Sigma_{F_c}}{z_{UV}}].\end{aligned} \tag{50}$$

One can also see the equivalence between the KK picture in the limit $z_{IR} \to +\infty$ and the continuum picture by comparing the differential decay rate for large z_{IR} in the KK picture versus the continuum case where one still keeps the particle behavior for the initial gluino state, but replaces the final state squark phase space, by an unparticle phase space [2].

For that purpose, let us calculate the continuum squark phase space for $c \neq 1/2$ and $c = 1/2$. In order to get the phase space of the squark final state, we calculate first the spectral function $\rho(p^2) = 2 \cdot \mathrm{Im}(i\Delta(p^2))$, where $\Delta(p^2)$ is the squark correlator whose expression was calculated in Ref. [1]. As was done in previous calculations, we are interested in the case when the momenta involved are much bigger than the squark's

mass gap, $p \gg \mu_f$. Using the expressions of the correlator in the limit when $pz_{UV} \ll 1$ we then find that for $-1/2 < c < 1/2$,

$$\rho(p^2) = \frac{2B(p^2)}{A(p^2)^2 + B(p^2)^2}, \tag{51}$$

where

$$\begin{aligned} A(p^2) &= \frac{p^2\epsilon^{1-2c}}{1-2c} - \frac{2^{-1+2c}p^2(p^2-\mu_f^2)^{-1/2+c}\cos(\pi(-\frac{1}{2}+c))\Gamma(1-2c)\Gamma(c)}{\Gamma(2c)\Gamma(1-c)}, \\ B(p^2) &= -\frac{2^{-1+2c}p^2(p^2-\mu_f^2)^{-1/2+c}\sin(\pi(-\frac{1}{2}+c))\Gamma(1-2c)\Gamma(c)}{\Gamma(2c)\Gamma(1-c)}, \end{aligned} \tag{52}$$

and that for $c = 1/2$,

$$\rho(p^2) = \frac{2 \cdot \frac{\pi}{2}}{(\gamma_E + \log(\frac{\epsilon}{2}\sqrt{p^2-\mu_f^2}))^2 p^2 + \frac{\pi^2}{4}p^2}. \tag{53}$$

The continuum squark phase space is then given by,

$$d\Phi_{\tilde{e}} = \theta(p^0)\theta(p^2-\mu_f^2)\rho(p^2), \tag{54}$$

where $\theta(p)$ is the Heaviside step function. On the other hand, the phase space for the outgoing quark is just the usual particle one,

$$d\Phi_e = 2\pi\theta(p^0)\delta(p^2). \tag{55}$$

With all this information, we are ready to calculate the 2-body phase space integral. [4] Let us name the momentum of the incoming gluino as $p_{\tilde{g}}$, and of the outgoing quark and squark momenta as p_u and $p_{\tilde{u}}$. Then the 2-body phase space integral is given by

$$\Pi_2 = \int (2\pi)^4\delta^{(4)}(p_{\tilde{g}} - p_{\tilde{u}} - p_u)2\pi\delta(p_u^2)\theta(p_u^0)\rho(p_{\tilde{u}}^2)\theta(p_{\tilde{u}}^0)\theta(p_{\tilde{u}}^2-\mu_f^2)\frac{d^4p_u}{(2\pi)^4}\frac{d^4p_{\tilde{u}}}{(2\pi)^4}. \tag{56}$$

We can perform the integral over the part of the quark phase space using that,

$$\int 2\pi\delta(p_u^2)\theta(p_u^0)\frac{d^4p_u}{(2\pi)^4} = \int \frac{d^3p_u}{(2\pi)^3 2E_u}\bigg|_{p_u^0>0}. \tag{57}$$

[4] Even though the vertex depends on the momenta of the particles, it only ends up depending on the quark energy E_u and the initial gluino energy $p_{\tilde{g}}^0$.

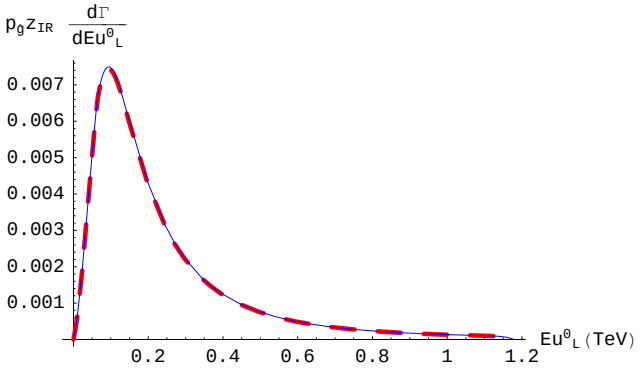

Figure 9: We use $z_{UV} = 10^{-3}$ TeV^{-1}, $z_{IR} = 80$ TeV^{-1}, $c = 0.5$ and $g_5 = 0.108$TeV$^{-1/2}$ and fix $p_{\tilde{g}} = 2.40$ TeV, $\mu_g = 0.2$ TeV, and $\mu_f = 0.3$ TeV. The plots compare the continuum method (red dashed curve) with the KK mode method (blue curve), they are almost identical.

Using the 4-dimensional delta function to perform the integrals over $d^4p_{\tilde{u}}$ and in the center of mass frame (CM) of the gluino, we can trivially perform the angular integration, $d^3p_u = E_u^2 dE_u d\Omega$, so that we obtain,

$$\Pi_2 = \frac{1}{2\pi^2}\frac{E_u^2}{2E_u}\rho((p^0_{\tilde{g}})^2 - 2p^0_{\tilde{g}}E_u)\theta((p^0_{\tilde{g}})^2 - 2p^0_{\tilde{g}}E_u - \mu_f^2)dE_u. \tag{58}$$

Once we have the expression for the phase space integral, we can write the differential decay rate as,

$$d\Gamma = \frac{|\mathcal{M}|^2}{2p^0_{\tilde{g}}}\Pi_2. \tag{59}$$

Averaging over the initial and summing over the final spin and color, we find that

$$|\mathcal{M}|^2 = 2|\tilde{c}(p^0_{\tilde{g}}, E_u, c)|^2 p^0_{\tilde{g}}E_u \mathrm{tr}[t^a t^a]/8 \ , \tag{60}$$

where

$$\tilde{c}(p^0_{\tilde{g}}, E_u, c) = \frac{1}{z_{UV}^{1/2}} \cdot \frac{c(p^0_{\tilde{g}}, E_u, c)}{\tilde{f}(q, z_{UV})} \ , \tag{61}$$

is the 4D effective vertex obtained from integrating over the profiles in 5D, divided by the normalized squark profile evaluated at the UV brane, and multiplied by $\frac{1}{z_{UV}^{1/2}}$ to be dimensionless, with $c(p^0_{\tilde{g}}, E_u, c)$ shown in Eq. (22). Thus we arrive at the formula,

$$\frac{d\Gamma_2}{dE_u} = \frac{E_u^2}{4\pi^2}|\tilde{c}(p^0_{\tilde{g}}, E_u, c)|^2 \rho((p^0_{\tilde{g}})^2 - 2p^0_{\tilde{g}}E_u)\theta((p^0_{\tilde{g}})^2 - 2p^0_{\tilde{g}}E_u - \mu_f^2). \tag{62}$$

In Fig 9 we plot the KK differential decay rate, Eq. (24), and the continuum decay rate, Eq. (62), as a function of the final quark energy E_u. They are in excellent agreement for large enough z_{IR}.

References

[1] H. Cai, H. C. Cheng, A. D. Medina and J. Terning, "Continuum Superpartners from Supersymmetric Unparticles," Phys. Rev. D **80**, 115009 (2009) hep-ph:0910.3925.

[2] H. Georgi, "Unparticle physics," Phys. Rev. Lett. **98** (2007) 221601, hep-ph/0703260.

[3] H. Georgi, "Another Odd Thing About Unparticle Physics," Phys. Lett. **B650** (2007) 275-278, hep-ph/0704.2457.

[4] P. J. Fox, A. Rajaraman and Y. Shirman, "Bounds on Unparticles from the Higgs Sector," Phys. Rev. **D76** (2007) 075004, hep-ph/0705.3092.

[5] G. Cacciapaglia, G. Marandella and J. Terning, "Colored Unparticles," JHEP **0801** (2008) 070, hep-ph:0708.0005.

[6] J. M. Maldacena, "The large N limit of superconformal field theories and supergravity," Adv. Theor. Math. Phys. **2**, 231 (1998) [Int. J. Theor. Phys. **38**, 1113 (1999)] hep-th/9711200; S. S. Gubser, I. R. Klebanov and A. M. Polyakov, "Gauge theory correlators from non-critical string theory," Phys. Lett. B **428**, 105 (1998) hep-th/9802109. E. Witten, "Anti-de Sitter space and holography," Adv. Theor. Math. Phys. **2**, 253 (1998) hep-th/9802150.

[7] G. Cacciapaglia, G. Marandella and J. Terning, "The AdS/CFT/Unparticle Correspondence," JHEP **0902** (2009) 049, hep-ph:0804.0424.

[8] M. J. Strassler, "Why Unparticle Models with Mass Gaps are Examples of Hidden Valleys," hep-ph:0801.0629.

[9] J. Polchinski and M. J. Strassler, "Deep inelastic scattering and gauge/string duality," JHEP **0305**, 012 (2003) hep-th/0209211]

[10] D. M. Hofman and J. Maldacena, "Conformal collider physics: Energy and charge correlations," JHEP **0805**, 012 (2008) hep-th:0803.1467.

[11] C. Csaki, M. Reece, J. Terning, "The AdS/QCD Correspondence: Still Undelivered," JHEP **0905** (2009) 067. hep-ph:0811.3001.

[12] M. A. Stephanov, "Deconstruction of Unparticles," Phys. Rev. **D76** (2007) 035008. hep-ph:0705.3049.

[13] D. Marti and A. Pomarol, "Supersymmetric theories with compact extra dimensions in $\mathcal{N} = 1$ superfields," Phys. Rev. D **64**, 105025 (2001) hep-th/0106256.

[14] L. Randall, R. Sundrum, "An Alternative to compactification," Phys. Rev. Lett. **83** (1999) 4690-4693. hep-th/9906064.

[15] A. Falkowski and M. Perez-Victoria, "Holographic Unhiggs," Phys. Rev. **D79** (2009) 035005, hep-ph:0810.4940; A. Falkowski, M. Perez-Victoria, "Electroweak Precision Observables and the Unhiggs," JHEP **0912** (2009) 061. hep-ph:0901.3777.

[16] J. B. G. da Costa *et al.* [Atlas Collaboration], "Search for squarks and gluinos using final states with jets and missing transverse momentum with the ATLAS detector in $\sqrt{s} = 7$ TeV proton-proton collisions," Phys. Lett. B **701**, 186 (2011) hep-ex:1102.5290; ATLAS-CONF-2011-086.

[17] V. Khachatryan *et al.* [CMS Collaboration], "Search for Supersymmetry in pp Collisions at 7 TeV in Events with Jets and Missing Transverse Energy," Phys. Lett. B **698**, 196 (2011) hep-ex:1101.1628.

[18] S. Chatrchyan *et al.* [CMS Collaboration], "Inclusive search for squarks and gluinos in pp collisions at $\sqrt{s} = 7$ TeV," hep-ex:1107.1279.